Journal Name

ARTICLE

Proton-Switchable Vapochromic Behaviour of a Platinum(II)-Carboxy-Terpyridine Complex

Received 00th January 20xx,
Accepted 00th January 20xx

DOI: 10.1039/x0xx00000x

www.rsc.org/

Atsushi Kobayashi,* Shiori Oizumi, Yasuhiro Shigeta, Masaki Yoshida and Masako Kato*

We synthesized a carboxy-substituted Pt(II)-terpyridine complex, i.e., [PtCl(Hctpy)]Cl (**[1H]Cl**; Hctpy = 4′-carboxy-2,2′:6′,2′′-terpyridine), that shows interesting *switchable* vapochromic behaviour upon protonation/deprotonation of the carboxy group. As-synthesized dark-blue amorphous-like solid **[1H]Cl**·3H_2O was converted to a yellow crystalline solid, **[1H]Cl**·H_2O, upon exposure to various polar organic solvent vapours (e.g., acetonitrile, ethanol, 1-propanol, and dichloromethane), which promote the removal of water molecules. The reaction of **[1H]Cl**·3H_2O with aqueous ammonia afforded a deprotonated bright-yellow crystalline complex, i.e., [PtCl(ctpy)]·H_2O (**1**·H_2O), which exhibits red luminescence with an emission maximum at 622 nm. Although the colour of **1**·H_2O was not affected by exposure to various polar organic solvent vapours, interesting vapochromic luminescence with a remarkable red-shift of the emission maximum from 622 to 652 nm was observed upon exposure to saturated water vapour to form orange crystalline **1**·3.5H_2O. X-ray structural analysis revealed that the planar and neutral complex molecule **1** forms a one-dimensional columnar structure with intermolecular Pt···Pt distances of 3.518(2) Å in the orange crystalline **1**·3.5H_2O, while the cationic molecule **[1H]**$^+$ in the protonated form, **[1H]Cl**·H_2O, generates a dimeric structure with an intermolecular Pt···Pt distance of 3.439(2) Å. This difference suggests that the vapochromic behaviours of the protonated and deprotonated forms could be caused by structural changes induced by water-vapour adsorption/desorption, which affect the intermolecular Pt···Pt distance, thereby changing the energy of the metal-metal-to-ligand charge-transfer (MMLCT) transition. These contrasting results for the protonated and deprotonated complexes clearly indicate that the hydrophilicity of complex **1** is significantly affected by protonation/deprotonation of the carboxy group. In addition, quasi-reversible conversion between **[1H]Cl**·3H_2O and **1**·H_2O was achieved by exposure of the protonated and deprotonated forms to triethylamine and humid hydrochloric acid vapours, respectively.

Introduction

Chromic materials showing reversible colour change in response to various external stimuli (e.g., temperature, pressure, and chemical vapour) have drawn increasing attention recently because of their potential applications in a variety of physical and chemical sensors. Especially, vapochromic materials that exhibit reversible colour change in response to harmful volatile organic chemical (VOC) vapours have been extensively studied for use in chemical sensors to detect such harmful chemicals in our environment.[1-5] The colour and luminescence of square-planar Pt(II) complexes strongly depend on their stacking orientation in the solid state, which directly affects the intermolecular metallophilic interactions between adjacent Pt(II) ions (i.e., modifies the metal-metal-to-ligand charge transfer (MMLCT) transition);[6-8] therefore, many vapochromic complexes, including simple neutral mononuclear complexes,[9-20] ionic complexes,[21-30] double salts,[31-34] dinuclear complexes,[35-38] and coordination polymers,[39-41] have been reported. Most of the vapochromism of Pt(II) complexes reported to date originates from reversible structural transformations induced by vapour adsorption/desorption, which changes the molecular stacking in the solid state. In addition to the intermolecular metallophilic interactions of Pt(II) ions, other intermolecular interactions (e.g., π–π stacking and hydrogen-bonding interactions) also play important roles in the chromic behaviour of Pt(II) complexes. For example, Chen *et al.* reported the dramatic vapochromic behaviour of a bisphenylacetylide Pt(II) complex, i.e., [Pt($Me_3SiC{\equiv}C$bpy$C{\equiv}CSiMe_3$)($C{\equiv}CPh$)$_2$] (($Me_3SiC{\equiv}C$bpy$C{\equiv}C$-$SiMe_3$ = 5,5′-bis(trimethyl-silylethynyl)-2,2′-bipyridine; C≡CPh = 2,2′-bipyridine-5-acetylide), in response to various organic solvent vapours; these drastic responses were attributed to weak intermolecular C–H···π and/or π–π interactions.[13,15] Eisenberg and co-workers also reported the methanol vapour–induced vapochromic behaviour of a Pt(II)-terpyridine complex containing a hydrogen-bonding amide group, [PtCl(Nttpy)]$(PF_6)_2$ (Nttpy = 4′-(p-nicotinamide-*N*-

[a] *Department of Chemistry, Faculty of Science, Hokkaido University, North-10 West-8, Kita-ku, Sapporo, Hokkaido 060-0810, Japan; e-mail: akoba@sci.hokudai.ac.jp (A.K.), mkato@sci.hokudai.ac.jp (M.K.)*

†Electronic Supplementary Information (ESI) available: X-Ray crystallographic data in CIF format; UV-Vis IR, ^{1}H NMR spectra, PXRD pattern, and thermogravimetric analysis results of **1H**-Cl·3H_2O; PXRD pattern of **1**·H_2O. See DOI: 10.1039/x0xx00000x

methylphenyl)-2,2′:6′,2′′-terpyridine).[22,30] The amide group forms double hydrogen bonds with the same group of the adjacent molecule to support a one-dimensional stacked structure with effective intermolecular Pt···Pt interactions. We also reported a vapochromic Pt(II) complex bearing both hydrogen-bond donating and accepting groups, i.e., $[Pt(CN)_2(H_2dcbpy)]$ (H_2dcbpy = 4,4′-dicarboxy-2,2′-bipyridine), and recently discovered that the complex and its derivative, $[Pt(CN)_2(H_2dcphen)]$ ($H_2dcphen$ = 4,7-dicarboxy-1,10-phenanthroline), exhibit interesting vapochromic behaviour with a shape-memory effect in which the two-dimensional hydrogen-bonding network plays an important role.[11,20] These reports clearly indicate the importance of exploiting hydrogen-bonding interactions for the design of new vapochromic Pt(II) complexes. However, most of the vapochromic behaviours of Pt(II) complex systems are derived from modification of the crystal structure without any changes in the molecular structure of the Pt(II) complex molecule; the exceptions involve significant changes to the coordination environment of the Pt(II) centre.[9,18] For example, a Pt(II)-diimine complex with ambidentate thiocyanato (SCN^-) ligands, i.e., $[Pt(H_2dcbpy)(thiocyanato)_2]$, exhibits vapochromic behaviour that involves vapour-induced linkage isomerization of the ambidentate thiocyanato ligand.[18].

Recently, we have focused on protonation/deprotonation of the hydrogen-bonding carboxy group because the protonated carboxylic acid group can act as both a proton-donating and -accepting group while the deprotonated carboxylate is a strong proton-accepting group; this difference could be exploited to affect the crystal packing of the planar Pt(II) complex molecules. In fact, we have already reported the significantly different crystal structures of Pd(II) complexes with protonated and deprotonated hydrazone ligands, which only have one protonation site.[42,43] The results of these early studies motivated us to investigate the effect of protonation/deprotonation of the carboxy groups attached to planar Pt(II) complex systems. Herein, we report switchable vapochromic behaviour upon protonation/deprotonation of the carboxy group of a novel Pt(II)-terpyridine complex, i.e., [PtCl(Hctpy)]Cl (Scheme 1, **[1H]Cl**; Hctpy = 4′-carboxy-2,2′:6′,2′′-terpyridine). In this complex, the carboxy group is directly attached to the 4′-position of the highly planar terpyridine ligand; therefore, the protonation/deprotonation reaction should affect the stacking of the planar Pt(II)-terpyridine complex molecules. In fact, the protonated complex, **[1H]Cl**, shows vapochromic behaviour upon dehydration by exposure to polar organic solvent vapours, while the deprotonated complex, [PtCl(ctpy)] (**1**), exhibits vapochromism driven by water-vapour adsorption. We also demonstrate that protonation/deprotonation of the carboxy group of **1** can be successfully and quasi-reversibly achieved by exposure to humid HCl/triethylamine vapours.

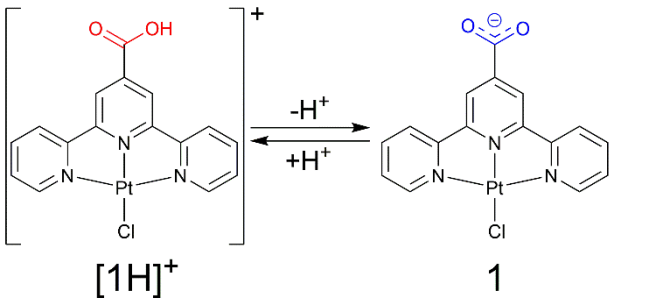

Scheme 1. Schematic molecular structures of the protonated **[1H]**$^+$ and deprotonated (**1**) forms.

Experimental Section

Synthetic Procedures.

Caution! *Although we experienced no difficulties, most of chemicals used in this study are potentially harmful and should be used in small quantities and handled with care in a fume hood.* All commercially available starting materials were used without purification. The starting materials, terpyridine ligand, i.e., Hctpy (4′-carboxy-2,2′:6′,2′′-terpyridine), and $[PtCl_2(COD)]$ (COD = 1,5-cyclooctadiene) were prepared according to literature methods.[45,46].

Synthesis of the Protonated Complex, [PtCl(Hctpy)]Cl·3H$_2$O ([1H]Cl·3H$_2$O). $[PtCl_2(COD)]$ (204 mg, 545 μmol) and Hctpy (140 mg, 501 μmol) were suspended in H_2O (25 mL). The reaction mixture was stirred overnight at 65 °C, and then the solvent was removed by evaporation under vacuum. The resultant deep-blue precipitate was collected by filtration, washed using a small amount of dichloromethane (20 mL), and dried under vacuum. Yield: 215 mg (360 μmol, 72%). Elemental analysis calcd for $C_{16}H_{11}Cl_2N_3O_2Pt·3H_2O$: C 32.17, H 2.87, N 7.03. Found: C 32.00, H 2.83, N 7.08. ^{1}H NMR (DMSO-d^6, 298 K) δ 8.02 (dd, 2H), 8.53 (dd, 2H), 8.93 (d, 2H), 9.02 (s+d, 4H).

Synthesis of the Deprotonated Complex, [PtCl(ctpy)]·H$_2$O (1). Powdered **[1H]Cl**·3H_2O (50 mg, 83.7 μmol) was dissolved in 7% NH_3 aq. (12 mL). Diffusion of CH_3COOH vapour into the solution for four days afforded orange crystals. The crystals were isolated by filtration, washed with a small amount of water, and dried under vacuum to give a bright yellow crystalline powder. Yield: 35 mg (66.7 μmol, 70%). Elemental analysis calcd for $C_{16}H_{10}ClN_3O_2Pt·H_2O$: C 36.62, H 2.30, N 8.01. Found: C 36.82, H 2.37, N 8.17. ^{1}H NMR (4% ND_3 in D_2O, 298 K) δ 7.89 (dd, 2H), 8.44 (br, 4H), 8.56 (s, 2H), 8.65 (d, 2H).

Preparations of Single Crystals.

Orange crystals of deprotonated 1·3.5H$_2$O. [1H]Cl·3H_2O (3 mg, 5.0 μmol) was dissolved in a solvent mixture comprising water (3.6 mL) and triethylamine (TEA; 0.4 mL). Slow diffusion of HCl gas from 3 M HCl aqueous solution into the solution at 30 °C for 10 days afforded orange crystals of **1**·3.5H_2O. One of the single crystals was used for X-ray structural analysis.

Yellow crystals of protonated [1H]Cl·H$_2$O. [1H]Cl·3H_2O (1.4 mg, 2.3 μmol) was dissolved in *N,N*-dimethylformamide (DMF). After filtration, slow diffusion of HCl gas from 8 M HCl aqueous solution into the filtrate at 30 °C for 12 days afforded yellow

Table 1. Crystal parameters and refinement data

Complex	**1**·3.5H_2O	**[1H]Cl**·H_2O
T / K	173(1)	100(1)
Formula	$C_{16}H_{10}ClN_3O_2Pt·3.5H_2O$	$C_{16}H_{11}Cl_2N_3O_2Pt·H_2O$
Formula weight	578.88	561.29
Crystal System	monoclinic	Triclinic
Space group	$P2_1/a$	*P*-1
a / Å	6.925(5)	7.463(6)
b / Å	17.917(13)	9.743(6)
c / Å	14.788(11)	13.044(10)
α / deg	90	69.55(4)
β / deg	100.119(10)	80.84(4)
γ / deg	90	69.53(3)
V / Å^3	1806(2)	831.8(11)
Z	4	2
D_{cal} / g·cm^{-3}	2.095	2.241
Reflections collected	16104	7132
Unique reflections	3789	4010
GOF	1.053	1.022
R_{int}	0.0965	0.0435
R_1(I) [a]	0.0540	0.0351
wR_2 [b]	0.1427	0.0913

[a] $R_1 = \Sigma||F_o| - |F_c||/\Sigma|F_o|$. [b] $wR_2 = [\Sigma w(F_o^2 - F_c^2)/\Sigma w(F_o)^2]^{1/2}$, $w = [\sigma_c^2(F_o^2) + (xP)^2 + yP]^{-1}$, $P = (F_o^2 - 2F_c^2)/3$.

crystals of **[1H]Cl**·H_2O. One of the single crystals was used for X-ray structural analysis.

Measurements.

Elemental analysis was performed at the Analysis Centre of Hokkaido University. ^{1}H NMR spectra were obtained using a JEOL EX270 NMR spectrometer. UV-Vis spectra were obtained in solution using a Shimadzu UV-2400PC spectrophotometer. Diffuse reflectance spectra were obtained using the same spectrometer equipped with an integrating sphere apparatus. The reflectance spectra were converted to absorption spectra using the Kubelka-Munk function. Luminescence and IR spectra were obtained using a JASCO FP-6600 spectrometer at room temperature and JASCO FT/IR spectrometer, respectively. Powder X-ray diffraction (PXRD) was conducted using either a Rigaku SPD diffractometer at beamline BL-8B at the Photon Factory, KEK, Japan or a Bruker D8 Advance diffractometer equipped with a graphite monochromator using Cu Kα radiation and a one-dimensional LinxEye detector. The wavelength of the synchrotron X-ray was 1.5385(1) Å. Thermogravimetry and differential thermal analysis were performed using a Rigaku ThermoEvo TG8120 analyzer. Vapour adsorption isotherms were obtained using BELSORP-max vapour adsorption isotherm measurement equipment.

Single-Crystal X-Ray Structural Analysis.

All measurements were performed using a Rigaku AFC-11 diffractometer with a Mercury CCD area detector at beamline PF-AR NW2A at the Photon Factory, KEK, Japan. The wavelength of the synchrotron X-rays was 0.6890(1) Å. All single crystals were mounted onto a MicroMount coated with paraffin oil. The crystal was then cooled using an N_2 flow–type temperature controller. Diffraction data were collected and processed using the CrystalClear program.[47] Structures were solved by the direct method using SIR-2011.[48] Structural refinements were conducted using the full-matrix least-squares method using SHELXL-2013.[49] The non-H atoms were refined anisotropically, and the H atoms were refined using the riding model. All calculations were performed using the Crystal Structure crystallographic software package.[50] The crystallographic data obtained for each complex are summarized in Table 1. Selected bond lengths and angles are listed in Table 2. Full crystallographic data were deposited with the Cambridge Crystallographic Data Centre (CCDC 1498641-1498642).

Table 2. Selected bond lengths (Å) and angles (°) for **1**·3.5H_2O and **[1H]Cl**·H_2O

	1·3.5H_2O	**[1H]Cl**·H_2O
Pt(1)–N(1)	2.032(8)	2.031(5)
Pt(1)–N(2)	1.947(8)	1.949(7)
Pt(1)–N(3)	2.023(8)	2.020(5)
Pt(1)–Cl(1)	2.314(3)	2.307(2)
C(16)–O(1)	1.245(15)	1.218(9)
C(16)–O(2)	1.243(14)	1.315(7)
N(1)–Pt(1)–N(2)	81.9(3)	81.1(2)
N(2)–Pt(1)–N(3)	81.2(3)	81.32)
N(1)–Pt(1)–N(3)	163.0(3)	162.4(3)
N(2)–Pt(1)–Cl(1)	178.8(2)	179.07(15)
O(1)–C(16)–O(2)	127.7(9)	125.5(7)

Results and discussion

Crystallography.

Single crystals of the deprotonated complex, i.e., **1**·3.5H_2O, were successfully obtained by acid-base neutralization of the deep-blue protonated complex, i.e., **[1H]Cl**·3H_2O, in triethylamine aqueous solution using HCl vapour, because the solubility of **[1H]Cl**·3H_2O to neutral or acidic aqueous solution is very low whereas it easily dissolved in basic aqueous solution. Thus, in this crystallization process, most of HCl molecules reacted with basic triethylamine to neutralize the solution and did not give the proton to the complex **1**. Fig. 1 shows the crystal structure of **1**·3.5H_2O. The central Pt(II) ion adopts a square-planar geometry in which the three N atoms of the ctpy ligand and one Cl ion occupy the four coordination sites. The Pt(1)–N(2) bond length of the central pyridyl ring is the shortest among the three Pt–N bonds (see Table 2). The Pt–Cl and Pt–N bond lengths and N(1)–Pt(1)–N(3) bond angle were very similar to those of the non-substituted Pt-terpyridine complexes,[51-54] suggesting that the introduction of the carboxy group into the 4′-position of terpyridine ligand does not significantly affect the coordination structure of the central Pt(II) ion. The two C–O bond lengths of the carboxy group (1.245(15) and 1.243(14) Å) are almost equivalent, indicating that the group was deprotonated to an anionic carboxylate. As a result, the complex molecule **1** is neutral, which is consistent with the absence of a counter anion in the

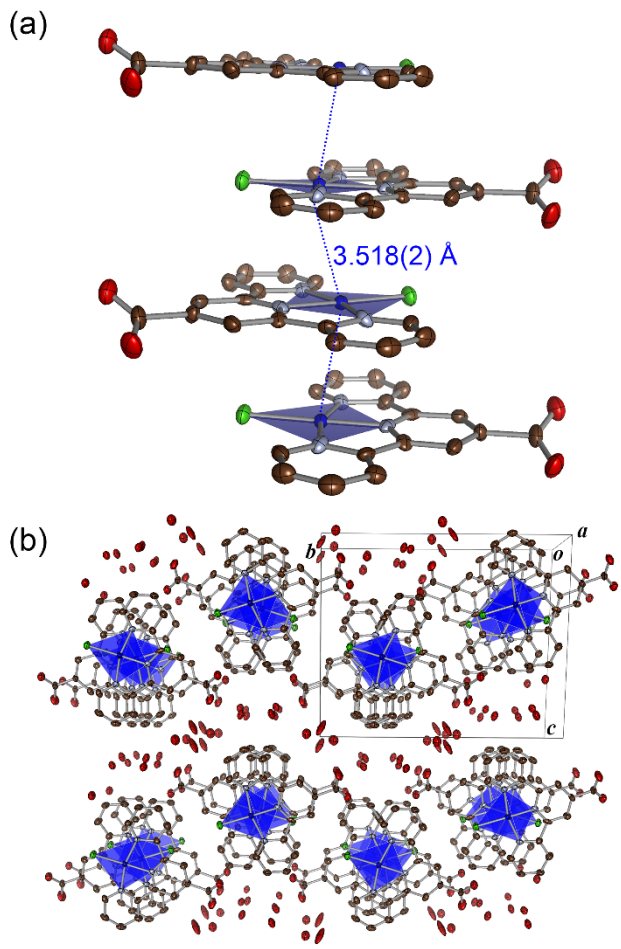

Fig. 1. (a) One-dimensional stacking and (b) packing structures of **1**·3.5H_2O. The coordination plane of the Pt(II) ion is shown in blue. The blue, green, brown, light-blue, and red ellipsoids represent Pt, Cl, C, N, and O atoms, respectively. The H atoms are omitted for clarity. Displacement parameters are drawn at a 50% probability level.

crystal structure. The large torsion angle between the carboxylate group and coordination plane of the central Pt(II) ion (28.18°) suggests that the two O atoms of the carboxylate are outside the square-planar coordination plane of the Pt(II) ion. Three water molecules are hydrogen-bonded to the negatively charged O atoms of the carboxylate with distances ranging from 2.70(1) to 2.77(2) Å. One of the three water molecule was disordered at the two sites with quarter occupancies near the midpoint between two adjacent complex molecules (see Fig. S1). The other water molecule is hydrogen-bonded to the other water molecules rather than the O atoms of the carboxylate. As shown in Fig. 1(a), the neutral complex molecules form a one-dimensional stacked structure with intermolecular Pt···Pt distances (3.518(2) Å) that are comparable to twice the van der Waals radius of Pt (3.5 Å); this stacking structure suggests intermolecular Pt···Pt and/or π-π interactions would be effective. The layer-by-layer structure formed from the alternating arrangement of one-dimensional columns of the neutral Pt(II) complex and hydrated water molecules is clearly evident along the *c* axis, as shown in Fig. 1(b).

The protonated form was obtained via acidification of a DMF solution of **[1H]Cl**·3H_2O by HCl vapour deposition from an 8 M HCl aqueous solution. The determined crystal structure is shown in Fig. 2. The central Pt(II) ion adopts a square-planar geometry via coordination to three N atoms of the ctpy ligand and the Cl ligand, and the Pt–N and Pt–Cl bond distances are similar to those of **1**·3.5H_2O, as shown in Table 2. In contrast, the two C–O bonds in the carboxy group differ significantly, indicating the presence of a carboxylic acid group. Thus, the effect of protonation/deprotonation of the carboxy group on the coordination structure of the central Pt(II) ion is negligible. The torsion angle between the carboxy group and coordination plane of the Pt(II) ion (4.21°) is significantly smaller than that of **1**·3.5H_2O. As a result of the protonation of the carboxy group, the charge of the Pt(II) complex molecule is +1; this is consistent with the presence of the counter Cl^- anion, which is hydrogen-bonded to the protonated carboxylic acid group. The Cl···H–O distance (2.977(6) Å) is 0.15 Å shorter than the average distance (3.12 Å),[55,56] suggesting strong hydrogen-bonding interactions. In this complex, only one water molecule per Pt(II) complex molecule forms a hydrogen

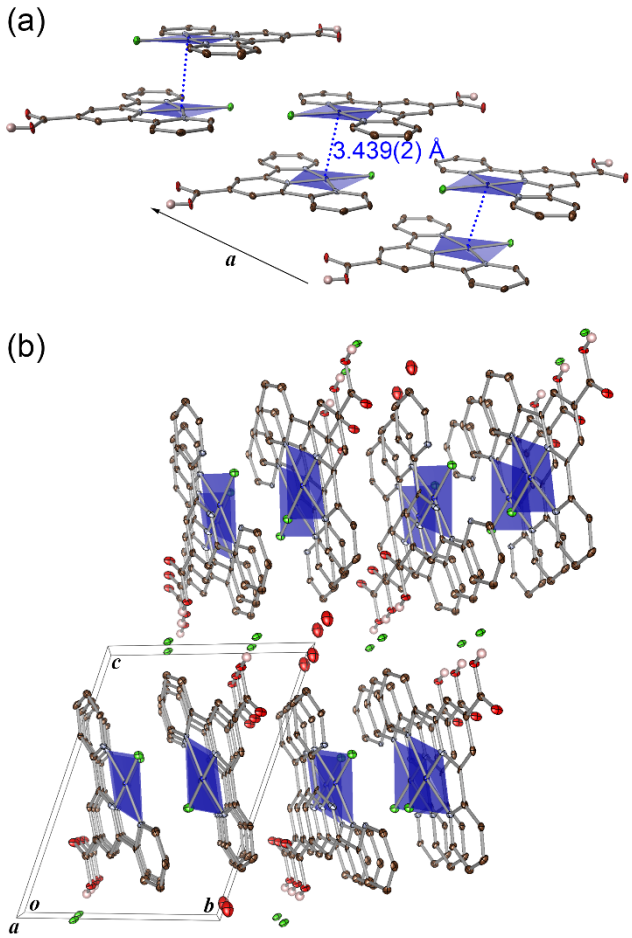

Fig. 2. (a) Stacking and (b) packing structures of (a) **[1H]Cl**·H_2O. The coordination plane of the Pt(II) ion is shown in blue. The blue, green, brown, light-blue, and red ellipsoids represent Pt, Cl, C, N, and O atoms, respectively. The H atoms bonded to the O atoms of the carboxy groups are shown as pink balls, and the others are omitted for clarity. Displacement parameters are drawn at a 50% probability level.

bond with the counter Cl^- anion. It should be noted that the cationic Pt(II) complex molecules formed a one-dimensional columnar stacked structure, as shown in Fig. 2(a); however, the intermolecular Pt···Pt distance in the column (7.145(4) Å) is too long for metallophilic interactions whereas the intermolecular Pt···Pt distance between the adjacent columns (3.439(2) Å) is sufficiently short for effective metallophilic interactions. Considering the fact that the interplanar distance (3.441 Å) is short enough for π–π stacking interactions, the cationic Pt(II) complex molecules form dimers in the crystal via intermolecular metallophilic and π–π stacking interactions. A similar layer-by-layer structure as that of **1**·3.5H_2O formed along the *c* axis by the alternate arrangement of cationic layers of the Pt(II) complex molecules and anionic layers of counter Cl^- anions with water molecules, as shown in Fig. 2(b).

Vapochromic Behaviour of Protonated Complex, [PtCl(Hctpy)]Cl.

Since the reaction between the Hctpy ligand and Pt(II) precursor complex [$PtCl_2$(COD)] afforded a unique dark-blue coloured powder, i.e., **[1H]Cl**·3H_2O, we investigated the vapochromic behaviour of this complex. Unfortunately, the crystallinity of this powder is very low, which made it difficult to determine the crystal structure; however, the intense band assignable to the C=O vibration mode at 1705 cm^{-1} in the IR spectrum is clear evidence of the protonated form (see Fig. S2). Elemental and thermogravimetric (TG) analyses for this dark-blue powder clearly indicated that three hydrated water molecules per one Pt complex were contained (see Experimental section and Fig. S3). Although the mixed-valent Pt complexes, so-called Platinum blues, are well-known complexes to exhibit characteristic blue colour in the solid state,[57-59] all ^{1}H signals of the ligand of **[1H]Cl**·3H_2O were clearly observed in ^{1}H NMR spectrum in DMSO-*d*^{6} solution (see Fig. S4), suggesting that the Pt centre was not in the paramagnetic mixed valent state. Thus, the dark blue powder obtained from the reaction between the Hctpy ligand and Pt(II) precursor complex [$PtCl_2$(COD)] should be the protonated trihydate complex, **[1H]Cl**·3H_2O. Fig. 3(a) shows the changes in the UV-vis diffuse reflectance spectra of **[1H]Cl**·3H_2O upon exposure to acetonitrile vapour at room temperature. **[1H]Cl**·3H_2O showed an intense and broad absorption band at around 650 nm; after exposure to acetonitrile vapour for three days, the colour changed from dark blue to yellow and the characteristic broad band completely disappeared. In addition, the initial dark-blue **[1H]Cl**·3H_2O was non-luminescent, but greenish-yellow emission was obviously observed after exposure to acetonitrile vapour (Fig. S5). Notably, the UV-vis diffuse reflectance spectrum of **[1H]Cl**·H_2O was almost identical to that of the complex after exposure to acetonitrile vapour; this suggests that the colour change from dark blue to yellow induced by exposure to acetonitrile vapour is caused by dehydration from **[1H]Cl**·3H_2O to **[1H]Cl**·H_2O. In fact, no peak assignable to adsorbed acetonitrile was observed in the IR or ^{1}H NMR spectra of the yellow powder (see Fig. S2 and S4) and elemental analysis for the yellow powder was well agreed with the calculated value of **[1H]Cl**·H_2O.[60] Considering that the yellow powder changed to a dark-blue powder upon exposure to saturated water vapour at 303 K for 10 days, the vapochromic change of protonated **[1H]Cl**·3H_2O from dark blue to yellow is due to dehydration by the highly hydrophilic acetonitrile vapour. Further, the UV-Vis absorption spectra of DMSO solutions of as-synthesized **[1H]Cl**·3H_2O and the yellow powder are almost identical to each other (Fig. S6), suggesting that the colour change from dark-blue to yellow in the solid state could originate from the modification of the crystal

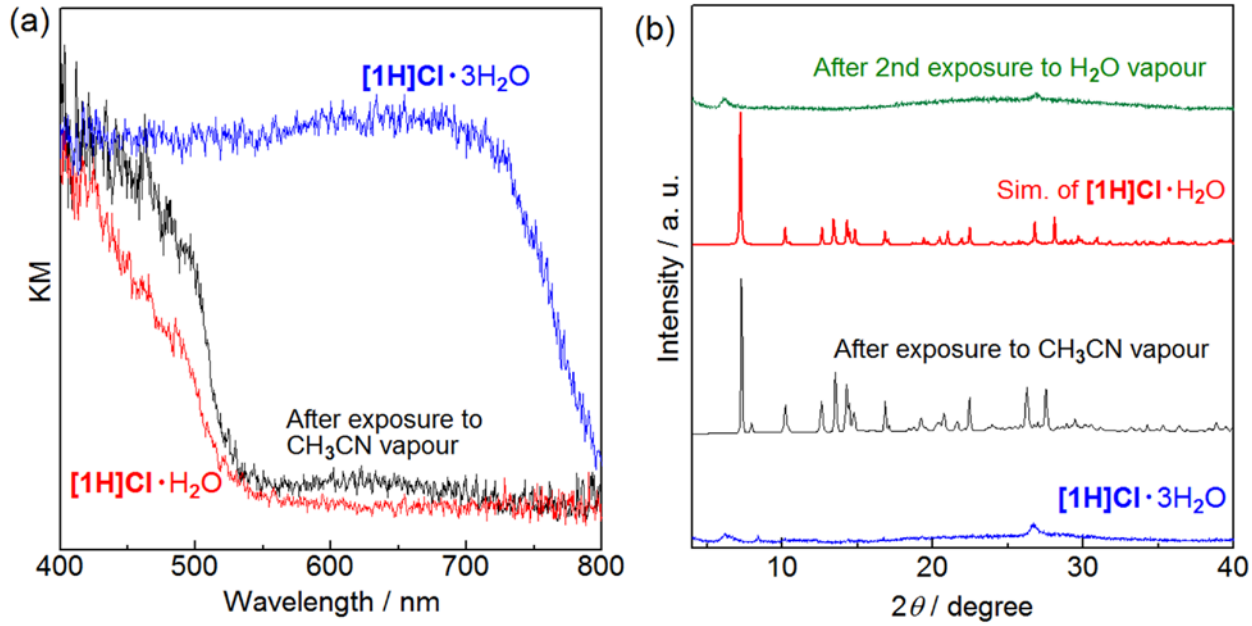

Fig. 3. Changes in the (a) UV-vis diffuse reflectance spectra and (b) PXRD patterns of **[1H]Cl**·3H_2O after exposure to CH_3CN vapour at 303 K for three days. The red lines in panels (a) and (b) show the spectra of **[1H]Cl**·H_2O and the simulation pattern calculated from the X-ray structure of **[1H]Cl**·H_2O, respectively. Upper and lower photographs in (a) show the bright field images of **[1H]Cl**·3H_2O before and after exposure to CH_3CN vapour. The green line in (b) shows the pattern obtained for the sample that was exposed to saturated H_2O vapour for 10 days at 303 K.

packing structure by exposure to acetonitrile vapour.

The vapochromic behaviour of the protonated form, **[1H]Cl**·3H_2O, upon exposure to acetonitrile vapour was also investigated by PXRD. As shown in Fig. 3(b), the pattern of the initially dark-blue **[1H]Cl**·3H_2O showed only a weak and broad peak at 6.2° and 26.7°, respectively, suggesting that **[1H]Cl**·3H_2O is almost amorphous. Interestingly, many sharp peaks were clearly evident after exposure to acetonitrile vapour, and the obtained PXRD pattern is almost identical to the simulated pattern of the yellow crystalline monohydrate, **[1H]Cl**·H_2O. These results indicate that dark-blue amorphous-like **[1H]Cl**·3H_2O was converted to the yellow crystalline monohydrate, **[1H]Cl**·H_2O. Similar changes to the PXRD patterns were observed upon exposure to ethanol, 1-propanol, and dichloromethane vapour; however, no changes were observed upon exposure to *n*-hexane or diethylether vapour (see Fig. S7 and S8). Thus, it is apparent that the vapochromism of **[1H]Cl**·3H_2O driven by adsorption/desorption of water vapour depends on the degree of hydrophilicity of the vapour.

We also investigated the thermal removal of the water in **[1H]Cl**·3H_2O because the dark-blue amorphous-like **[1H]Cl**·3H_2O was converted to the yellow crystalline monohydrate **[1H]Cl**·H_2O by hydrophilic vapour–induced dehydration. Thermogravimetric analysis revealed that all three water molecules were completely removed upon increasing the temperature to 393 K (see Fig. S3). However, it should be noted that the PXRD pattern remained the same in the temperature range of 298 to 393 K (see Fig. S9), and the sample remained dark blue after heating. Thus, in addition to dehydration, the molecules in the solid state must also rearrange to induce the conversion from the amorphous-like trihydrate **[1H]Cl**·3H_2O to the crystalline monohydrate **[1H]Cl**·H_2O. In other words, exposure to hydrophilic vapour may promote molecular rearrangement in the solid state more effectively than thermal treatment.

Vapochromic Behaviour of Deprotonated Complex, [PtCl(ctpy)].

The protonated complex, i.e., **[1H]Cl**·3H_2O, showed interesting vapochromic behaviour upon exposure to various hydrophilic organic vapours; therefore, we also investigated the vapochromic behaviour of the bright-yellow deprotonated form, **1**·H_2O, which was obtained via a neutralization reaction between the basic aqueous ammonia solution of **[1H]Cl**·3H_2O and acetic acid vapour. Although no colour change was observed in the presence of polar organic solvent vapours (e.g., acetonitrile and dichloromethane, see Fig. S10), an interesting colour change from bright yellow to orange was observed upon exposure of **1**·H_2O to saturated water vapour. Simultaneously, as shown in Fig. 4(a), the emission of the complex changed: **1**·H_2O exhibited luminescence centred at 621 nm; this was significantly red-shifted up to 652 nm upon exposure to water vapour. The resultant orange sample reverted to the initial bright-yellow **1**·H_2O upon exposure to dried air overnight at room temperature (see Fig. 4(a)), suggesting that the vapochromic luminescence of **1**·H_2O is due to reversible adsorption/desorption of water vapour. In fact, the PXRD pattern of the orange sample obtained after exposure of **1**·H_2O to water vapour is almost identical to the simulated pattern calculated from the more hydrated deprotonated form, **1**·3.5H_2O, as shown in Fig. 4(b). These results clearly indicate that **1**·H_2O shows vapochromic luminescence driven by adsorption/desorption of water vapour. As discussed in the crystal structure section, intermolecular metallophilic interactions are evident in **1**·3.5H_2O, suggesting that the orange emission centred at 652 nm of **1**·3.5H_2O could originate from an MMLCT. The bright yellow monohydrate, **1**·H_2O, had a higher emission energy

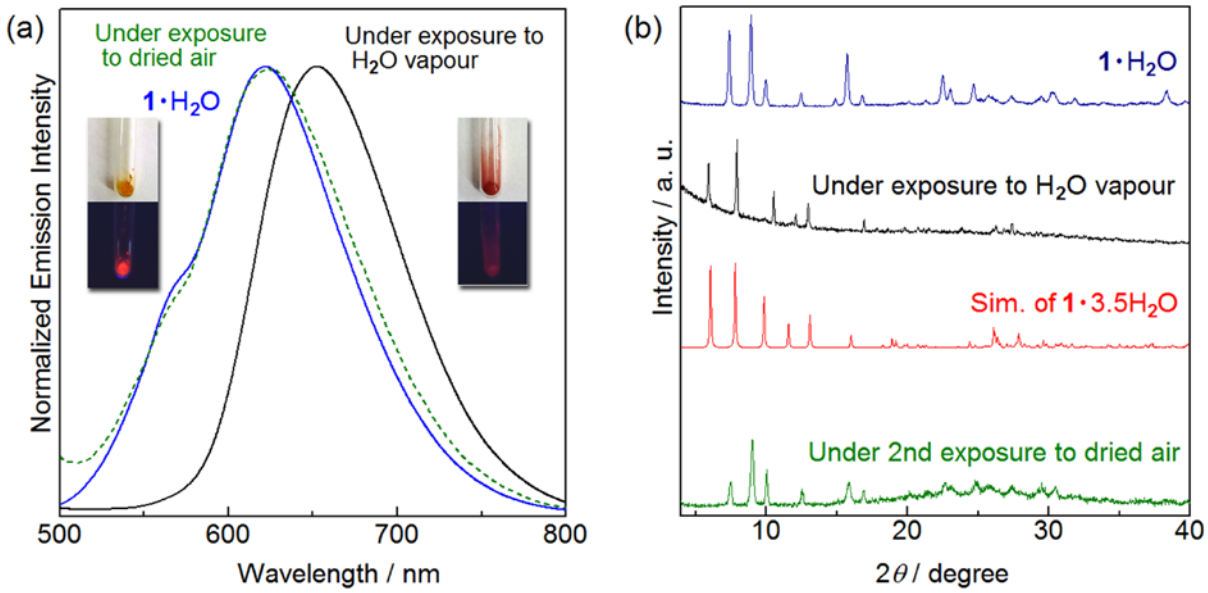

Fig. 4. Changes in the (a) luminescence spectra (λ_{ex} = 400 nm) and (b) PXRD patterns of **1**·H_2O (blue) upon exposure to saturated water vapour (black) and further exposure to dried air (green) at room temperature. The left- and right-side photographs in (a) show the (upper) bright field and (lower) luminescence images of **1**·H_2O before and after exposure to saturated water vapour. The red line in panel (b) shows the simulated pattern calculated from the X-ray structure of **1**·3.5H_2O.

than **1**·3.5H_2O, which suggests weaker intermolecular metallophilic interactions. In other words, the desorption of water molecules from the crystal lattice of **1**·3.5H_2O may induce the collapse of the one-dimensionally stacked structure of the planar Pt(II) complex molecules.

Hydrophilicity Control by Protonation/Deprotonation.

As discussed above, the vapochromic behaviour of complex **1** strongly depends on the protonation/deprotonation of the carboxy group attached to the 4′-position of the terpyridine ligand. The protonated form, i.e., **[1H]Cl**·3H_2O, shows vapochromic behaviour in response to hydrophilic organic vapours owing to dehydration, whereas the deprotonated form **1**·H_2O exhibits vapochromic luminescence driven by water vapour adsorption. These contrasting results suggest a large difference in the hydrophilicity of the protonated and deprotonated forms of complex **1**.

To elucidate the differences between the protonated and deprotonated forms, we measured their water vapour adsorption isotherms. As shown in Fig. 5, deprotonated **1** adsorbed water vapour in two steps: A small amount of water (~0.5 mol·mol^{-1} Pt(II) complex) was adsorbed in the low relative humidity region (below 0.1 P/P_0) and a large water vapour uptake (~3 mol·mol^{-1} Pt(II) complex) was observed at a very high humidity (above 0.9 P/P_0). The first water adsorption could be due to chemisorption driven by the formation of hydrogen bonds with the carboxylate group, as suggested by the X-ray structure of **1**·3.5H_2O. The wide plateau region from 0.1 to 0.9 P/P_0 suggests that high water vapour pressure is required for the second water adsorption step in order to induce the structural change to the fully hydrated form of **1**·3.5H_2O. The saturated amount of water uptake (3.5 mol·mol^{-1} Pt(II) complex) is quantitatively consistent with the X-ray structural analysis results. In the desorption process, three desorption steps were observed: The first desorption occurred at 0.69 P/P_0 with large hysteresis to form the trihydrate form, the second desorption occurred as a sharp decrease at 0.57 P/P_0 to form the monohydrate form of **1**·H_2O, and the third desorption to form anhydrous **1** was observed below 0.05 P/P_0. The large hysteresis for the second water vapour adsorption/desorption at high humidity also suggests that significant structural changes are required for this water-adsorption process. On the other hand, the protonated form of **[1H]Cl** showed a completely different adsorption isotherm: Water adsorption continually increased over all vapour pressure ranges, and the wide plateau observed for deprotonated **1** was not observed. As shown in Fig. 5, three different adsorption processes are clearly evident: The first step occurs from 0 to 0.7 P/P_0 to form the trihydrated form, the second step formed the tetrahydrated form in the region of 0.7 < P/P_0 < 0.9, and the third step involved a remarkable steep increase at high humidity (above 0.9 P/P_0). The maximum amount of water adsorption was 6 mol·mol^{-1}, which is significantly larger than that of the deprotonated form of **1**. In the desorption process, the same three steps that were observed in the adsorption process were evident with hysteresis.

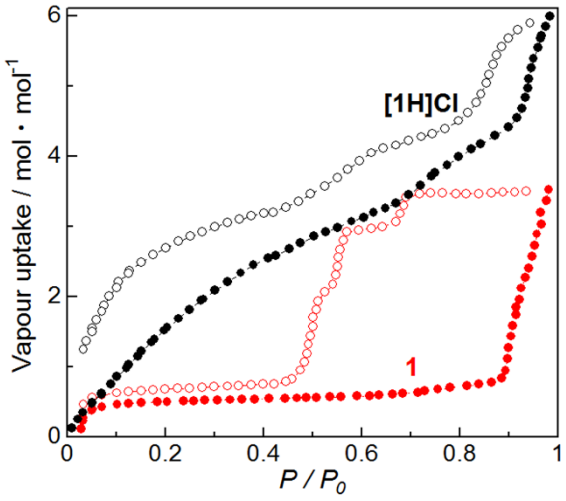

Fig. 5. Water-vapour isotherms of **1** (red) and **[1H]Cl** (black) at 298 K. Closed and open symbols indicate adsorption and desorption, respectively.

The completely different isotherms of the protonated **[1H]Cl** and deprotonated **1** clearly indicate the effect of protonation of the carboxyl group: Protonation of the carboxy group enhanced the hydrophilicity of the complex because of the positive charge of the molecule, counter Cl^- anion, and changes in the hydrogen-bonding nature of the carboxy group. The higher hydrophilicity of the protonated **[1H]Cl** as compared to that of deprotonated **1** caused **[1H]Cl** to exhibit vapochromic behaviour originating from dehydration under hydrophilic organic vapours, whereas the less hydrophilic **1** only showed vapochromic luminescence upon exposure to saturated water vapour.

Interconversion by Exposure to Acidic/Basic Vapours.

As mentioned above, the vapochromic behaviour of the complex **1** strongly depends on the protonation/deprotonation state of the carboxy group. This remarkable difference motivated us to investigate interconversions between the protonated and deprotonated forms using some acidic and basic vapours. In this section, we discuss interconversions driven by humid HCl and TEA as the acidic and basic vapours, respectively.

The bright-yellow deprotonated form, **1**·H_2O, converted to a dark-blue powder upon exposure to humid HCl vapour at room temperature overnight. As shown in Fig. 6(a), the obtained dark-blue powder showed a broad absorption band at around 650 nm in the UV-vis diffuse reflectance spectrum, which is similar to that of the protonated **[1H]Cl**·3H_2O. In the IR spectra, the C=O vibration mode observed at 1625 cm^{-1} for **1**·H_2O dramatically shifted to a higher wavenumber of 1701 cm^{-1} upon exposure to humid HCl vapour (Fig. 6(b)), suggesting protonation of the carboxylate group. In addition, the dark-blue powder showed a very broad PXRD pattern with small peaks at 6.2° and 26.7°, which are characteristic for the protonated amorphous-like **[1H]Cl**·3H_2O (Fig. S11). From these

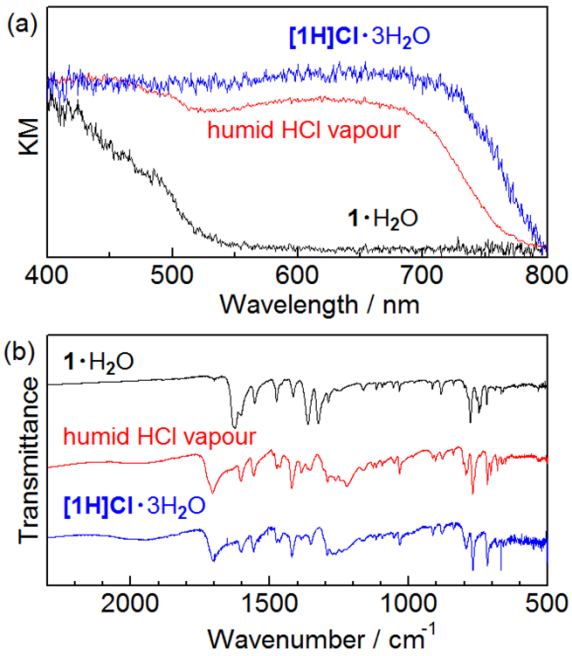

Fig. 6. Changes in the (a) UV-vis diffuse reflectance and (b) IR spectra of **1**·H_2O (dark blue) upon exposure to humid HCl vapour at room temperature. The blue line in each panel shows the spectrum of **[1H]Cl**·$3H_2O$.

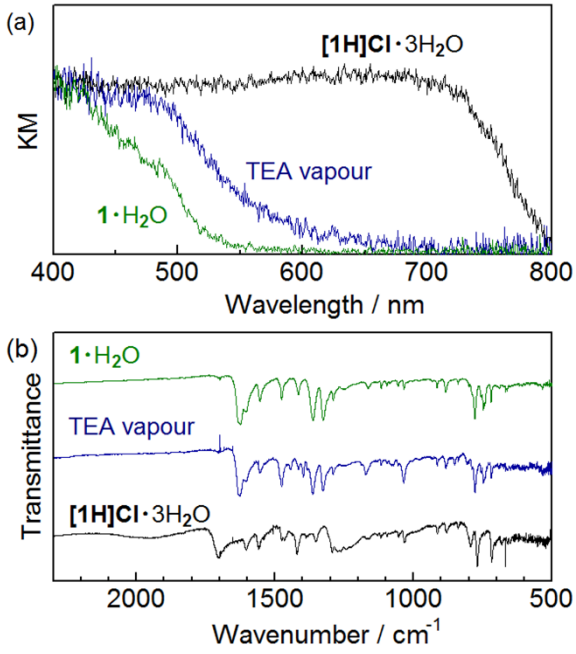

Fig. 7. Changes in the (a) UV-vis diffuse reflectance and (b) IR spectra of **[1H]Cl**·$3H_2O$ (black) upon exposure to basic triethylamine (TEA) vapor at room temperature. The green line in each panel shows the spectrum of **1**·H_2O.

results, we conclude that the conversion from **1**·H_2O to **[1H]Cl**·$3H_2O$ can be achieved by exposure of the deprotonated form to humid HCl vapour. On the other hand, different colour change from the bright-yellow to pale yellow was observed under exposing **1**·H_2O to humid nitric or acetic acid vapour (Fig. S13). Sharp diffraction peaks were clearly observed in the PXRD patterns of these pale yellow samples, and IR spectral changes suggest that the protonation of the carboxylate group of **1** occurred under exposure to nitric acid, while it seems to be remained as the deprotonated state after exposure to acetic acid vapour. This difference is probably due to the large difference of pKa value between these two acids. These results also suggest that not only the protonation of the carboxylate group of **1** but also the shape of anion are important for the dark-blue color of **[1H]Cl**·$3H_2O$. In other words, the sphere shape of Cl^- anion, which can randomly form several hydrogen bonds with proton-donating groups, may contribute to the formation of dark-blue amorphous form of **[1H]Cl**·$3H_2O$.

Next, we investigated the reverse interconversion from the protonated form, **[1H]Cl**·$3H_2O$, to the deprotonated form, **1**·H_2O, using TEA vapour as the base to remove the proton on the carboxylic acid group. It should be noted that the counter Cl^- anion of **[1H]Cl**·$3H_2O$ should also be removed in this process. Fig. 7(a) shows the change in the UV-vis diffuse reflectance spectrum of **[1H]Cl**·$3H_2O$ upon exposure to TEA vapour. After exposure for three days at 303 K, the solid changed from dark blue to bright yellow and the characteristic absorption band of the protonated form in the UV-vis diffuse reflectance spectrum at around 650 nm clearly disappeared. Simultaneously, the C=O vibration mode appeared at 1632 cm^{-1} in the IR spectrum, and the spectrum was qualitatively identical to the spectrum of **1**·H_2O after exposure to TEA vapour (Fig. 7(b)); these results suggest that the carboxylic acid group was deprotonated to form **1**·nH_2O. The small difference between the UV-vis diffuse reflectance spectra of the deprotonated form, **1**·H_2O, and the bright yellow powder might be due to a different number of hydrated water molecules. On the other hand, two characteristic signals (i.e., 1.0 and 2.5 ppm) for TEA were clearly observed in the aliphatic region of the ^1H NMR spectrum of the bright yellow powder (see Fig. S12), and their signal intensities suggest that there is one TEA molecule per Pt(II)-terpyridine complex. Thus, the interconversion from **[1H]Cl**·$3H_2O$ to **1**·nH_2O occurred by exposure to TEA vapour, which reacts with the proton on the carboxylic acid group of **1H** to form **1** and a triethylammonium chloride (Et_3NHCl) byproduct.

Conclusions

We newly synthesized a Pt(II)-terpyridine complex, i.e., [PtCl(Hctpy)]Cl (**[1H]Cl**; Hctpy = 4′-carboxy-2,2′:6′,2″-terpyridine), which possesses a carboxy functional group as the protonation/deprotonation site to control the vapochromic behaviour. The protonated trihydrate form, **[1H]Cl**·$3H_2O$, showed a dramatic vapochromic response (from dark blue to yellow) upon exposure to various hydrophilic organic vapours (e.g., alcohols, acetonitrile, dichloromethane, etc.), which likely occurs due to desorption of the water molecules to form the protonated monohydrate form, **[1H]Cl**·H_2O. Although this vapochromic behaviour originates from reversible water desorption/adsorption, negligible

changes in both the colour of the solid and PXRD pattern were observed after drying by heating, suggesting that the vapours may promote molecular rearrangement in the crystal packing. X-ray analysis clearly indicated that intermolecular metallophilic interactions are effective in the π–π stacked dimer in **[1H]Cl**·H_2O. On the other hand, the bright-yellow deprotonated form, (**1**·H_2O), did not show any vapochromic behaviour in the presence of various organic solvent vapours; however, it did exhibit interesting vapochromic luminescence upon exposure to saturated water vapour to form orange **1**·3.5H_2O, which comprised a one-dimensionally stacked columnar structure with moderate intermolecular metallophilic interactions. Interconversions between the protonated and deprotonated forms were also achieved by exposure to humid HCl or triethylamine vapour as the proton-donating or -accepting vapours, respectively. Since the water-vapour adsorption isotherms clearly indicate that the protonated form, **[1H]Cl**, is significantly more hydrophilic than the deprotonated form, **1**, protonation/deprotonation could be one of the most useful strategies for the design of multifunctional chemical sensing molecular devices.

Acknowledgements

This study was supported by JST-PRESTO, Shimadzu Science Foundation, Shorai Science and Technology Foundation, Inamori Foundation, Murata Science Foundation, Grant-in-Aid for Scientific Research (C)(26410063) and Artificial Photosynthesis (No. 2406) from MEXT, Japan.

Notes and references

1 O. S. Wenger, *Chem. Rev.*, 2013, **113**, 3686–3733.
2 M. Kato, *Bull. Chem. Soc. Jpn.*, 2007, **80**, 287–294.
3 A. Kobayashi, and M. Kato, *Eur. J. Inorg. Chem.*, 2014, 4469–4483.
4 X. Zhang, B. Li, Z.-H. Chen, and Z.-N. Chen, *J. Mater. Chem.*, 2012, **22**, 11427–11441.
5 M. Mauro, A. Aliprandi, D. Septiadi, N. Seda Kehr, and L. De Cola, *Chem. Soc. Rev.*, 2014, **43**, 4144–4166.
6 V. M. Miskowski, and V. H. Houlding, *Inorg. Chem.*, 1989, **28**, 1529–1533.
7 V. M. Miskowski, and V. H. Houlding, *Inorg. Chem.*, 1991, **30**, 4446–4452.
8 J. A. Bailey, M. G. Hill, R. E. Marsh, V. M. Miskowski, W. P. Schaefer, and H. B. Gray, *Inorg. Chem.*, 1995, **34**, 4591–4599.
9 M. Albrecht, M. Lutz, A. L. Spek, and G.-v. Koten, *Nature*, 2000, **406**, 970–974.
10 C. E. Buss, and K. R. Mann, *J. Am. Chem. Soc.*, 2002, **214**, 1031–1039.
11 M. Kato, S. Kishi, Y. Wakamatsu, Y. Sugi, Y. Osamura, T. Koshiyama, and M. Hasegawa, *Chem. Lett.,* 2005, **34**, 1368–1369.
12 J. Ni, Y. H. Wu, X. Zhang, B. Li, L. Y. Zhang, and Z.-N. Chen, *Inorg. Chem.*, 2009, **48**, 10202–10210.
13 J. Ni,L.-Y. Zhang, H.-M. Wen, and Z.-N. Chen, *Chem. Commun.*, 2009, 3801–3803.
14 J. Ni, X. Zhang, N. Qiu, Y. H. Wu, L. Y. Zhang, J. Zhang, and Z.-N. Chen, *Inorg. Chem.*, 2011, **50**, 9090–9096.
15 J. Ni, X. Zhang, Y.-H. Wu, L.-Y. Zhang, and Z.-N. Chen, *Chem. Eur. J.* 2011, **17**, 1171–1183.
16 X. Zhang, J. Y. Wang, J. Ni, L.-Y. Zhang, and Z.-N. Chen, *Inorg. Chem*., 2012, **51**, 5569–5579.
17 S. J. Choi, J. Kuwabara, Y. Nishimura, T. Arai, and T. Kanbara, *Chem. Lett.*, 2012, **41**, 65–67.
18 A. Kobayashi, Y. Fukuzawa, H.-C. Chang, and M. Kato, *Inorg. Chem.*, 2012, **51**, 7508–7519.
19 N. Kitani, N. Kuwamura, T. Tsuji, K. Tsuge, and T. Konno, *Inorg. Chem.*, 2014, **53**, 1949–1951.
20 Y. Shigeta, A. Kobayashi, T. Ohba, M. Yoshida, T. Matsumoto, H.-C. Chang, and M. Kato, *Chem. Eur. J.,* 2016, **22**, 2682–2690.
21 L. J. Grove, J. M. Rennekamp, H. Jude, and W. B. Connick, *J. Am. Chem. Soc.*, 2004, **126**, 1594–1595.
22 T. J. Wadas, Q.-M. Wang, Y.-j. Kim, C. Flaschenreim, T. N. Blanton, and R. Eisenberg, *J. Am. Chem. Soc.,* 2004, **126**, 16841–16849.
23 P. Du, J. Schneider, W. W. Brennessel, and R. Eisenberg, *Inorg. Chem.*, 2008, **47**, 69–77.
24 L. J. Grobe, A. G. Oliver, J. A. Krause, and W. B. Connick, *Inorg. Chem.*, 2008, **47**, 1408–1410.
25 M. L. Muro, C. A. Daws, and F. N. Castellano, *Chem. Commun.*, 2008, 6134–6136.
26 J. Forniés, S. Fuertes, J. A. López, A. Martín, and V. Sicilia, *Inorg. Chem*., 2008, **47**, 7166–7176.
27 A. Kobayashi, T. Yonemura, and M. Kato, *Eur. J. Inorg. Chem.,* 2010, 2465–2470.
28 J. S. Field, C. D. Grimmer, O. Q. Munro, and B. P. Waldron, *Dalton Trans.,* 2010, **39**, 1558–1567.
29 C. S. Lee, R. R. Zhuang, S. Sabiah, J. C. Wang, W. S. Hwang, and I. J. B. Lin, *Organometallics*, 2011, **30**, 3897–3900.
30 A. Han, P. Du, Z. Sun, H. Wu, H. Jia, R. Zhang, Z. Liang, R. Cao, and R. Eisenberg, *Inorg. Chem.*, 2014, **53**, 3338–3344.
31 C. L. Exstrom, J. R. Jr. Sowa, C. A. Daws, D. Janzen, and K. R. Mann, *Chem. Mater.*, 1995, **7**, 15–17.
32 C. A. Daws, C. L. Exstrom, J. R. Jr. Sowa, and K. R. Mann, *Chem. Mater.*, 1997, **9**, 363–368.
33 C. L. Exstrom, M. K. Pomije, and K. R. Mann, *Chem. Mater.*, 1998, **10**, 942–945.
34 S. M. Drew, L. I. Smith, K. A. McGee, and K. R. Mann, *Chem. Mater.*, 2009, **21**, 3117–3124.
35 M. Kato, A. Omura, A. Toshikawa, S. Kishi, and Y. Sugimoto, *Angew. Chem. Int. Ed.*, 2002, **41**, 3183–3185.
36 S. C. F. Kui, S. S. Y. Chui, C. M. Che, and N. Zhu, *J. Am. Chem. Soc.*, 2006, **128**, 8297–8309.
37 T. Ohba, A. Kobayashi, H.-C. Chang, T. Koyama, T. Kato, and M. Kato, *Dalton Trans.*, 2014, **43**, 7514–7521.
38 T. Ohba, A. Kobayashi, H.-C. Chang, and M. Kato, *Dalton Trans.*, 2013, **42**, 5514–5523.
39 A. Kobayashi, H. Hara, S. Noro, and M. Kato, *Dalton Trans.*, 2010, **39**, 3400–3406.
40 H. Hara, A. Kobayashi, S. Noro, H.-C. Chang, and M. Kato, *Dalton Trans.*, 2011, **40**, 8012–8018.
41 A. Kobayashi, H. Hara, T. Yonemura, H.-C. Chang, and M. Kato, *Dalton Trans.*, 2012, **41**, 1878–1888.
42 A. Kobayashi, M. Dosen, M. Chang, K. Nakajima, S. Noro, and M. Kato, *J. Am. Chem. Soc.*, 2010, **132**, 15286–15298.
43 M. Chang, H. Horiki, K. Nakajima, A. Kobayashi, H.-C. Chang, and M. Kato, *Bull. Chem. Soc. Jpn.*, 2010, **83**, 905–910.
44 M. Chang, A. Kobayashi, K. Nakajima, H.-C. Chang, and M. Kato, *Inorg. Chem.*, 2011, **50**, 8308–8317.
45 A. Stublla, and P. G. Potvisn, *Eur. J. Inorg. Chem.*, 2010, 3040–3050.
46 J. X. McDermott, J. F. White, and G. M. Whitesides, *J. Am. Chem. Soc.*, 1976, **98**, 6521–6528.
47 *CrystalClear*: Molecular Structure Corporation: Orem, UT, 2001.
48 *SIR2011*: M. C. Burla, R. Caliandro, M. Camalli, B. Carrozzini, G. L. Cascarano, C. Giacovazzo, M. Mallamo, A. Mazzone, G. Polidori, and R. Spagna, *J. Appl. Cryst*., 2012, **45**, 357–361.

49 *SHELXL2013*: G. M. Sheldrick, *Acta Cryst*., 2008, **A64**, 112–122.
50 *CrystalStructure 4.1*: Crystal Structure Analysis Package; Rigaku Corporation: Tokyo, Japan, 2000–2014.
51 J. A. Bailey, M. G. Hill, R. E. Marsh, V. M. Miskowski, W. P. Schaefer, and H. B. Gray, *Inorg. Chem.*, 1995, **34**, 4591–4599.
52 H.-K. Yip, L.-K. Cheng, K.-K. Cheung, and C.-M. Chem, *J. Chem. Soc. Dalton Trans.*, 1993, 2933–2938.
53 S. D. Taylor, W. Howard, N. Kaval, R. Hart, J. A. Krause, and W. B. Connick, *Chem. Commun.*, 2010, **46**, 1070–1072.
54 C. S. Angle, A. G. DiPasquale, A. L. Rheingold, and L. H. Doerrer, *Acta Cryst.*, 2006, **C62**, m340–m342.
55 G. C. Pimental, and A. L. McClellan, *The Hydrogen Bond*; Freeman; San Francisco, 1960.
56 L. N. Kuleshova, and P. M. Zorkii, *Acta Cryst.*, 1981, **B37**, 1363–1366.
57 J. K. Barton, D. J. Szalda, H. N. Rabinowitz, J. V. Waszczak, and S. J. Lippard, *J. Am. Chem. Soc.*, 1979, **101**, 1434-1441.
58 K. Matsumoto, and K. Fuwa, *J. Am. Chem. Soc.*, 1982, **104**, 897-898.
59 K. Sakai, Y. Tanaka, Y. Tsuchiya, K. Hirata, T. Tsubomura, S. Iijima, and A. Bhattacharjee, *J. Am. Chem. Soc.*, 1998, **120**, 8366-8379.
60 Elemental analysis of the yellow powder. Found: C 34.08, H 2.33, N 7.49. Calcd for $C_{16}H_{11}Cl_2N_3O_2Pt{\cdot}H_2O$: C 34.24, H 2.34, N 7.51.